

Characterization of reactive oxidized nitrogen in the global upper troposphere using recent and historic commercial and research aircraft campaigns and GEOS-Chem

5 Nana Wei¹, Eloise A. Marais¹, Gongda Lu^{1*}, Robert G. Ryan^{1**}, Bastien Sauvage²

¹ Department of Geography, University College London, London, UK.

² Laboratoire d'Aérodynamique, Université de Toulouse, CNRS, Université Toulouse III Paul Sabatier, France.

* Now at: the Satellite Application Center for Ecology and Environment, Ministry of Ecology and Environment, Beijing, China.

10 ** Now at: School of Geography, Earth and Atmospheric Science, University of Melbourne, Melbourne, Australia.

Correspondence to: Nana Wei (nana.wei.21@ucl.ac.uk); Eloise A. Marais (e.marais@ucl.ac.uk)

Abstract. Reactive oxidized nitrogen (NO_y) in the upper troposphere (UT) influences global climate, air quality, and tropospheric oxidants, but this is informed by limited knowledge of the relative contribution of individual
15 NO_y components in this undersampled layer. Here we use sporadic NASA DC-8 aircraft campaign observations, after screening for plumes and stratospheric influence, to characterise UT NO_y composition and evaluate current knowledge of UT NO_y as simulated with the GEOS-Chem model. Use of DC-8 data follows confirmation that these intermittent data reproduce NO_y seasonality from routine commercial aircraft observations (2003-2019), supporting use of DC-8 data to characterize UT NO_y. We find that peroxyacetyl nitrate (PAN) dominates UT NO_y
20 (30-64% of NO_y), followed by nitrogen oxides (NO_x ≡ NO + NO₂) (6-18%), peroxyacetic acid (HNO₄) (6-13%), and nitric acid (HNO₃) (7-11%). Methyl peroxy nitrate (MPN) makes an outsized contribution to NO_y (14-24%) over the Southeast US relative to the other regions sampled (2-7%). GEOS-Chem, sampled along DC-8 flights, exhibits much weaker seasonality than DC-8, underestimating summer and spring NO_y and overestimating winter and autumn NO_y. The model consistently overestimates peroxypropionyl nitrate (PPN) by ~10-16 pptv or 10%-
25 90% and underestimates NO₂ by 6-36 pptv or 31%-65%, as the model is missing PPN photolysis. A model underestimate in MPN of at least ~50 pptv (13-fold) over the Southeast US results from uncertainties in processes that sustain MPN production as air ages. Our findings highlight that greater understanding of UT NO_y is critically needed to determine its role in the nitrogen cycle, air pollution, climate, and abundance of oxidants.

1 Introduction

30 Reactive oxidized nitrogen (NO_y) in the upper troposphere impacts global climate, surface air quality and the oxidizing capacity of the whole troposphere (Mickley et al., 1999; Bradshaw et al., 2000; Dahlmann et al., 2011; Worden et al., 2011). NO_y is an important climate driver because tropospheric ozone (O₃) production is limited by the availability of NO_y, particularly in the upper troposphere where the radiative forcing efficiency of O₃ peaks (Dahlmann et al., 2011; Worden et al., 2011; Rap et al., 2015). Influence on tropospheric O₃ production also
35 affects abundance of the main atmospheric oxidant, the hydroxyl radical (OH), thus altering the lifetimes of the longer-lived greenhouse gas methane and the air pollutants carbon monoxide (CO) and volatile organic compounds (VOCs) (Murray et al., 2013; Seltzer et al., 2015).

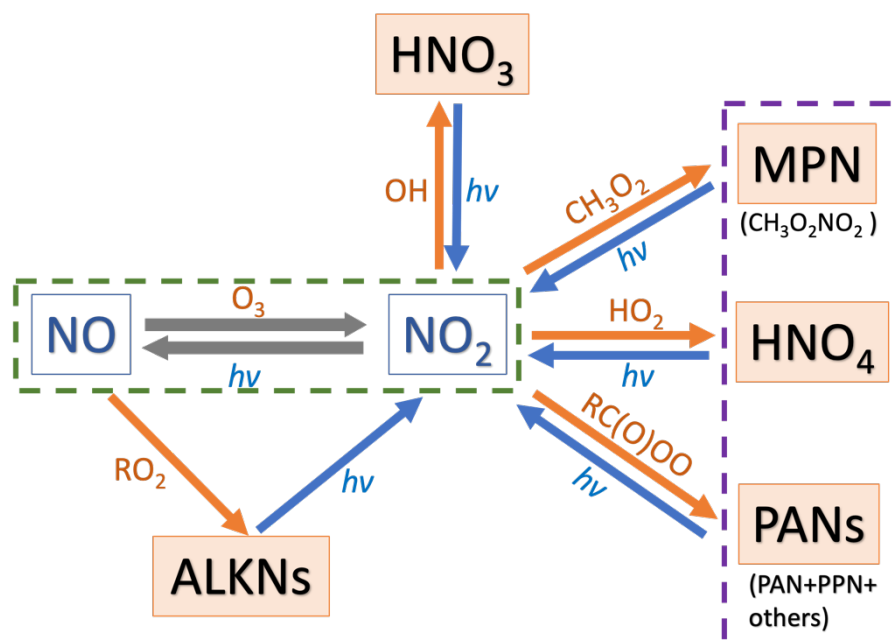
Knowledge of dominant daytime NO_y compounds, sources, chemistry, fate, and persistence in the upper troposphere has been largely informed by observations and models used as part of research and commercial aircraft campaigns (Boersma et al., 2011; Marais et al., 2018; Silvern et al., 2018; Travis et al., 2016; 2020). Instruments onboard research aircraft that sample the upper troposphere, in particular the recently retired NASA DC-8 platform, have undergone substantial development to directly measure and derive estimates of a large suite of upper tropospheric NO_y compounds. These include nitrogen oxides ($\text{NO}_x \equiv \text{NO} + \text{NO}_2$), peroxyacetyl nitrate (PAN) and other prominent PAN-type compounds, nitric acid (HNO_3), peroxyxynitric acid (HNO_4), alkylnitrates (ALKNs) and, more recently, methyl peroxy nitrate (MPN).

These aircraft campaigns have confirmed that sources of NO_y to the upper troposphere are dominated by lightning NO_x emissions (Levy II et al., 1999; Gressent et al., 2014; 2016; Marais et al., 2018), causing a seasonal maximum in NO_y in summer months and a minimum in winter in parts of the world such as the northern midlatitudes where there is large seasonal variability in lightning activity (Blakeslee et al., 2014; Stratmann et al., 2016). Other NO_y source contributors include NO_x emissions from cruising altitude aircraft (Brasseur et al., 1996), stratospheric downwelling of air masses laden with HNO_3 and NO_2 that also promote prompt formation of PANs on mixing with cold upper tropospheric air (Levy II et al., 1980; Jacob et al., 2010; Liang et al., 2011), deep convective uplift of surface pollution (Ehhalt et al., 1992; Jaeglé et al., 1998; Bertram et al., 2007), and aged air masses initially very photochemically active that accumulate MPN (Nault et al., 2015).

Chemical cycling of dominant daytime NO_y components, informed by past review and measurement compilation studies of the free troposphere (Emmons et al., 1997; Bradshaw et al., 2000), is illustrated in Figure 1. During the day, NO and NO_2 are in photostationary steady state, as NO oxidation, mostly by O_3 , is balanced by NO_2 photolysis. NO_x also reacts to form reservoir compounds. For NO_2 , these include HNO_3 from reaction with OH , PANs from reaction with peroxy acyl radicals ($\text{RC}(\text{O})\text{OO}$), HNO_4 from reaction with the hydroperoxyl radical (HO_2), and MPN from reaction with the methyl peroxy radical (CH_3O_2). PANs in the upper troposphere are typically dominated by PAN followed by peroxypropionyl nitrate (PPN) (Singh, 1987; Roberts, 1990; 1998; 2002). For NO , reservoir compounds include ALKNs from reaction with non-acyl peroxy radicals (RO_2). Recycling of reservoir compounds back to NO_x is dominated by photolysis, as thermally labile peroxy nitrates (PNs) including PANs, HNO_4 and MPN are stable against decomposition in the cold upper troposphere (Huey, 2007). This recycling along with NO_y sources to the upper troposphere sustains upper tropospheric NO_x concentrations at ~ 30 pptv over the remote ocean and ~ 100 pptv over polluted landmasses (Marais et al., 2018; 2021; Shah et al., 2023). Stable NO_x reservoir compounds are transported long distances before subsiding and decomposing on warming, thus supplying other parts of the world with oxidants (HO_x) and O_3 precursors (NO_x and peroxy radicals) (Schultz et al., 1999). Loss processes in the dry upper troposphere are slow and dominated by subsidence, resulting in long NO_y lifetimes of 10-20 days (Logan, 1983; Prather and Jacob, 1997). Similarly, NO_x has a lifetime of about a week compared to less than a day in the boundary layer (< 2 km) (Jaeglé et al., 1998).

Nighttime NO_y chemistry is also important, but aircraft campaign measurements of the nocturnal upper troposphere are mostly of total NO_y from commercial aircraft campaigns. The nighttime chemistry not in Figure 1 includes NO reaction with OH forming nitrous acid (HONO) that accumulates in the absence of photolysis, as

75 well as NO_2 reaction with O_3 to form the nitrate radical (NO_3) that further reacts with NO_2 to produce N_2O_5 , a precursor of aerosol nitrate (pNO_3) (Bradshaw et al., 2000).



80 **Figure 1: Dominant daytime reactive oxidized gas-phase nitrogen components and reaction pathways in the upper troposphere. Arrow colours distinguish formation (orange) and photolytic ($h\nu$) decomposition (blue) of reservoir compounds. Dashed boxes indicate compounds of the NO_x family (green) and classed as peroxy nitrates (purple). "R" in RC(O)OO and RO_2 represents an alkyl group.**

Modelling studies evaluating best understanding of NO_y in the upper troposphere routinely identify stark discrepancies between observed and modelled total NO_y , NO_x , and the ratio of NO -to- NO_2 in the upper layers of the troposphere (Jaeglé et al., 1998; Talbot et al., 1999; Bertram et al., 2007; Hudman et al., 2007; Liang et al., 2011; Nault et al., 2015; Huntrieser et al., 2016; Travis et al., 2016; Fisher et al., 2018; Silvern et al., 2018; Lee et al., 2022; Cohen et al., 2023). These studies have either focused on a few NO_y components, or a single aircraft campaign. A more holistic investigation of all NO_y components is needed, as is advocated by Murray et al. (2021), to reduce uncertainties in knowledge of the current, past, and potential future abundances of tropospheric oxidants. Past studies have also documented the challenges examining measurements made in the upper troposphere. These include screening for stratospheric influence, determining the height of the chemical tropopause, and selecting observations and campaigns that are climatologically representative of a standard atmosphere (Weinheimer et al., 1994; Fuelberg et al., 2000; Bertram et al., 2007; Barth et al., 2015; Huntrieser et al., 2016). Instruments measuring NO_2 are also susceptible to interference from decomposition of the least thermally stable NO_x reservoir compounds, HNO_4 and MPN , that are abundant in the cold upper troposphere (Ryerson et al., 2000; Shah et al., 2023). NO_y from these same instruments can also be biased by decomposition of non- NO_y fixed nitrogen compounds prevalent in the upper troposphere, such as hydrogen cyanide (HCN) (Bradshaw et al., 1998).

Here we use NASA DC-8 research and IAGOS commercial aircraft campaign measurements, each spanning more than a decade, to characterize global NO_y seasonality and composition in the upper troposphere. This follows careful campaign and data selection to isolate observations sampling the upper troposphere under standard

conditions for broad assessment of consistent NO_y seasonality between DC-8 and routine commercial aircraft campaign observations. We go on to use the DC-8 data to critique contemporary understanding of upper tropospheric NO_y as simulated by the GEOS-Chem model.

2 Materials and methods

2.1 Research aircraft observations of total and components of NO_y

The DC-8 research aircraft has sampled ambient air covering the near full extent of the troposphere since its maiden campaign in 1985 (Culter, 2009). Many of the initial campaigns included instruments that measured a subset of the NO_y components shown in Figure 1, typically continuous measurements of total NO_y , NO , HNO_3 , PAN and PPN, and whole air sampler (WAS) collection and laboratory detection of C1-C5 ALKNs (Singh et al., 1999). Since 2004, DC-8 campaigns have included continuous measurements of HNO_4 , other PAN-type species and total PNs (Singh et al., 2006). Given this, we only consider DC-8 campaigns with a relatively consistent suite of instruments that mostly sampled well-mixed air representative of a climatologically standard atmosphere. These criteria eliminate the summer 2004 Intercontinental Chemical Transport Experiment-North America (INTEX-NA) campaign (Singh et al., 2006; Singh et al., 2009) that is the only DC-8 campaign since 2004 to not include a NO_x and NO_y chemiluminescence analyzer, and the summer 2012 Deep Convective Clouds and Chemistry (DC3) campaign that targeted convective thunderstorms influenced by fresh surface pollution and lightning NO_x emissions (Barth et al., 2015).

The DC-8 campaigns we use are the Arctic Research of the Composition of the Troposphere from Aircraft and Satellites (ARCTAS) over the Arctic and sub-Arctic in spring and summer 2008 (Jacob et al., 2010), the Studies of Emissions and Atmospheric Composition, Clouds and Climate Coupling by Regional Surveys (SEAC⁴RS) over the Southeast US in late summer and early autumn 2013 (Toon et al., 2016), the Korea-United States Air Quality (KORUS-AQ) over South Korea in late spring and early summer 2016 (Crawford et al., 2021), and the Atmospheric Tomography Mission (ATom) that included 4 sub-campaigns along the same flight path from pole to pole over the Atlantic and Pacific Oceans in all 4 seasons from 2016 to 2018 (Thompson et al., 2021). ATom sub-campaigns are ATom-1 in July-August, ATom-2 in January-February, ATom-3 in September-October and ATom-4 in April-May. The data for these campaigns are from NASA data portals for each campaign downloaded as merged 1-minute files for ARCTAS (NASA, 2009), SEAC⁴RS (NASA, 2015) and KORUS-AQ (NASA, 2017) and as two separate merged files for ATom with the WAS C1-C5 ALKNs data at variable time intervals of 40 s, 1 min and 2 min and without the WAS C1-C5 ALKNs data at 1-minute resolution (NASA, 2021).

Figure 2 shows the global sampling extent of the upper troposphere by NASA DC-8 after applying filtering criteria to the data to isolate observations representative of photochemical steady-state conditions. For this, we select daytime (08h30-15h30 local solar time or LST) observations within a wide pressure range from 180 hPa (~8 km) to the DC8 ceiling of 450 hPa (~12 km). This captures the full vertical extent of the midlatitude upper troposphere, but not the tropics. The tropical tropopause, according to NASA Modern-Era Retrospective analysis for Research and Applications version 2 (MERRA-2) meteorology, extends to ~16 km. We separate the stratosphere from the troposphere with a tropopause definition that can be applied to all datasets. We remove data with observed O_3

concentrations above thresholds that represent the location of the chemical tropopause (Zahn et al., 2002). The thresholds we use are a single year-round value for the tropics (20°N to 20°S) of 100 ppbv (Dameris, 2015) and seasonally varying values everywhere else calculated using the day-of-year dependent O₃ tropopause equation derived by Zahn et al. (2002) from the inverse relationship between O₃ and CO observations from commercial aircraft campaigns. These are 120 ppbv in spring, 103 ppbv in summer, 74 ppbv in autumn, and 91 ppbv in winter. We also screen for stratospheric intrusions (identified as observations with O₃/CO > 1.25 mol mol⁻¹) (Hudman et al., 2007), fresh NO_x emissions (NO_y/NO < 3 mol mol⁻¹), fresh convection (large (> 10 nm diameter) condensation nuclei > 10⁴ cm⁻³), biomass burning plumes (CO > 200 ppbv and acetonitrile > 200 pptv) (Shah et al., 2023), as well as instances where NO₂ photolysis frequencies are approximately zero. The latter removes high latitude ATom measurements obtained at 08h30-15h30 LST under dark conditions during polar twilight or polar night. The data that are retained correspond to solar zenith angles ≤ 80° in polar regions, and ≤ 60° at other latitudes. The proportion of observations at 450-180 hPa is 42-50% for ATom and 16-37% for the other campaigns. After applying all other data screening, 20% of all data are retained for ATom and 7-11% for the other campaigns.

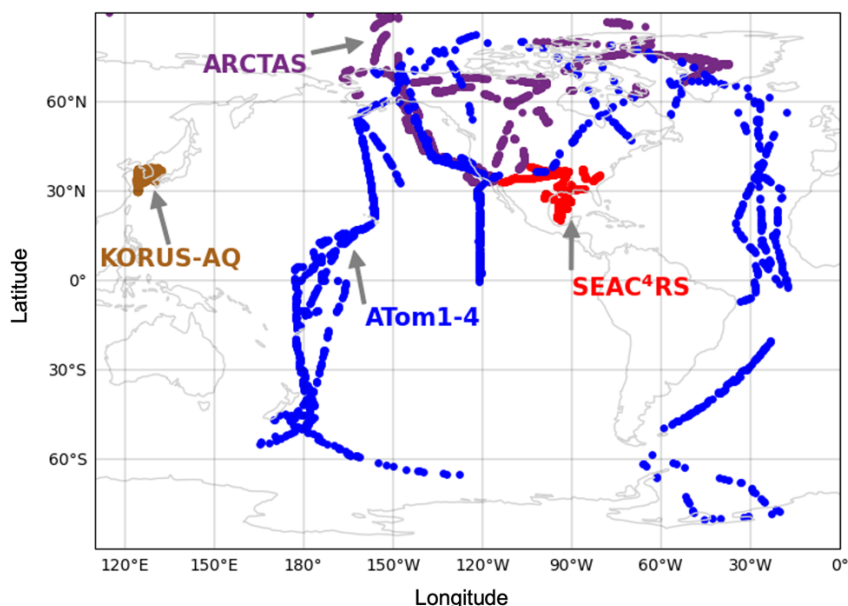


Figure 2: Extent of NASA DC-8 sampling of the upper troposphere under standard, steady-state conditions. Colours distinguish ARCTAS (plum), SEAC⁴RS (red), KORUS-AQ (brown), and ATom (blue). ATom points are the 1-minute resolution data.

The DC-8 instruments measuring NO_y components (Figure 1) that are common to all campaigns include a chemiluminescence instrument measuring NO, NO₂, and total NO_y (Ryerson et al., 2000; Pollack et al., 2010; Bourgeois et al., 2022), a chemical ionization mass spectrometer (CIMS) measuring HNO₃ (Crounse et al., 2006), a CIMS measuring HNO₄, PAN, PPN, and other PANs (Huey, 2007), and a Whole Air Sampler (WAS) collecting samples analysed in the laboratory using gas chromatography with flame ionization and atomic emission to detect C1-C5 ALKNs (Blake et al., 2003). The other PANs measured with the CIMS include peroxyacryloyl nitrate (APAN), peroxyisobutyryl nitrate (PiBN), peroxybutyryl nitrate (PBN), and peroxybenzoyl nitrate (PBZN). Other instruments deployed for select campaigns are Thermal-Dissociation Laser Induced Fluorescence (TD-LIF) measuring NO₂, total PNs and total ALKNs (ARCTAS, KORUS-AQ, SEAC⁴RS) (Day et al., 2002) and the PAN

and Trace Hydrohalocarbon Experiment (PANTHER) instrument measuring PAN (ATom). There are also TD-LIF methyl peroxy nitrate (MPN) measurements reported in the SEAC⁴RS dataset and derived for ARCTAS by Browne et al. (2011).

Concentrations of NO₂ in the upper troposphere are close to chemiluminescence instrument uncertainty (Pollack et al., 2010; Bourgeois et al., 2022) and the measurements include interference from decomposition of NO_x reservoir compounds in the instrument inlet. The Reed et al. (2016b) temperature-dependent inlet temperature decomposition profiles of individual NO_x reservoir compounds for an instrument similar to that operated on the DC-8 suggests interference of 80-100% MPN and 15-45% HNO₄ for the typical inlet temperature range of the DC-8 chemiluminescence instrument of 20-30°C (Bourgeois et al., 2022). For the campaigns that measured HNO₄ and derived or measured MPN, this amounts to 13-27 pptv for ARCTAS and 71-92 pptv for SEAC⁴RS. Given this, we instead calculate NO₂ using the NO-NO₂ photochemical steady state (PSS) approximation, as is now standard (Travis et al., 2016; Shah et al., 2023; Horner et al., 2024). Conversion of NO to NO₂, mostly (75%) due to oxidation by O₃ in the upper troposphere (Silvern et al., 2018), is balanced by NO₂ photolysis back to NO:



As NO_x is in steady state for the daylight observations we isolate, NO₂ can be calculated as follows:

$$\text{NO}_2 = \text{NO} \times \left(\frac{k_1[\text{O}_3] + k_2[\text{HO}_2] + k_3[\text{BrO}]}{j_{\text{NO}_2}} \right) \quad (1).$$

Compounds in square brackets are in molecules cm⁻³. NO and NO₂ are in pptv. Terms not introduced yet include the NO₂ photolysis frequency, j_{NO_2} , in s⁻¹, bromine monoxide (BrO), and rate constants of NO oxidation (R1) (k_{1-3}), in cm³ molecule⁻¹ s⁻¹. Temperature-dependent values of k_{1-3} are those recommended by the Jet Propulsion Laboratory (JPL) (Burkholder, 2020), calculated using DC-8 ambient temperature measurements. NO, [O₃], and j_{NO_2} are from the DC-8 measurements and [HO₂] is from the DC-8 measurements for all campaigns, except SEAC⁴RS when it was not measured. We use GEOS-Chem (detailed in Sect. 2.3) simulated [HO₂] to estimate SEAC⁴RS PSS NO₂. [BrO] is from GEOS-Chem for all campaigns. NO is also converted to NO₂ by organic peroxy radicals (RO₂), but we ignore this reaction as it is relatively insignificant throughout the free troposphere (Shah et al., 2023).

The NO_y components not measured during specific campaigns are inferred. These include HNO₄ for KORUS-AQ, and ATom-3-4, PPN for ATom-1-2, and MPN for ARCTAS, ATom-1-4 and KORUS-AQ. The approaches used to infer these values differs, informed by the results, so a detailed description of this inference is in Section 3.2.

2.2 Commercial aircraft observations of total NO_y

We use routine observations of upper tropospheric total NO_y from instruments on commercial long-haul passenger aircraft to determine if the intermittency and brevity of DC-8 campaign observations are representative of climatological conditions. The In-service Aircraft for a Global Observing System (IAGOS) European research infrastructure (Boulanger et al., 2018) provides routine in situ measurements of NO_y (Petzold et al., 2015). These are available from two IAGOS programmes: the Measurement of Ozone and Water Vapor by Airbus In-Service Aircraft (MOZAIC) (Marenco et al., 1998) from 2001 to 2005 (Volz-Thomas et al., 2005) and the Civil Aircraft for the Regular Investigation of the Atmosphere Based on an Instrument Container (CARIBIC) since December 2004 (Brenninkmeijer et al., 2007; Stratmann et al., 2016).

We consider the MOZAIC and CARIBIC observations together (collectively named IAGOS), as both programmes employed a chemiluminescence instrument with the same NO_y detection technique (Volz-Thomas et al., 2005; Brenninkmeijer et al., 2007). Direct intercomparison of NO_y is not possible, as there is no overlap in MOZAIC and CARIBIC NO_y. Data from 2003 to 2019 are used; 2003-2005 for MOZAIC and 2005-2019 for CARIBIC. We isolate daytime, upper tropospheric observations by applying the same O₃ tropopause, stratospheric O₃ intrusion, and daytime filtering as is applied to DC-8 data (Sect. 2.1) using IAGOS O₃ and CO measurements. There are no NO₂ photolysis frequency measurements, but the requirement for spatial coincidence with ATom excludes polar twilight and night measurements at high latitudes. We do not screen for observations impacted by fresh emissions, vertical convection or biomass burning plumes, due to unavailability of concurrent measurements of suitable chemical tracers in the IAGOS data. As we consider 17 years of IAGOS data, we assume that the influence of these is dampened in the long-term median of NO_y. Both the IAGOS and DC-8 data are gridded to the same 2° latitude × 2.5° longitude grid.

2.3 The GEOS-Chem Model

We use the GEOS-Chem global 3D chemical transport model version 13.0.2 (<https://doi.org/10.5281/zenodo.4681204>; last accessed May 2021) to represent contemporary understanding of upper tropospheric NO_y for comparison to DC-8. The model is driven with consistent MERRA-2 assimilated meteorology at 2° × 2.5° (latitude × longitude) over 47 vertical layers from the surface of the Earth to 0.01 hPa. The model emissions local to the upper troposphere include cruising altitude aircraft from the Aviation Emissions Inventory Code (AEIC) (Stettler et al., 2011) and lightning emissions as described in Murray et al. (2012). Surface emissions of NO_x and VOCs precursors of ALKNs and PN_s are from the anthropogenic Community Emissions Data System (CEDS) inventory of Hoesly et al. (2018), the Model of Emissions of Gases and Aerosols from Nature (MEGAN) biogenic VOCs inventory version 2.1 (Guenther et al., 2012), the soil NO_x emission inventory of Hudman et al. (2012), and the Global Fire Emissions Database version 4 with small fires (GFED4s) for open burning of biomass (Giglio et al., 2013). Wet deposition of gas-phase HNO₃, the terminal sink for NO_y subsiding from the upper troposphere, includes in-cloud (rainout) and below-cloud (washout) scavenging as detailed in Amos et al. (2012) and enhanced scavenging as described by Luo et al. (2020).

We sample the model at the same time and location as the DC-8 observations using the ObsPack diagnostic (<https://www.esrl.noaa.gov/gmd/ccgg/obspack/>; last accessed 23 October 2021) following a minimum 10-month spin-up preceding each campaign to initialize chemistry and large-scale circulation throughout the troposphere.

Modelled components of NO_y include NO , NO_2 , HNO_3 , HNO_4 , PAN, PPN, peroxyethacroyl nitrate (MPAN), MPN, and ALKNs.

3 Results and Discussion

245 3.1 DC-8 campaign NO_y seasonality and budget closure

Figure 3 compares seasonality in UT NO_y from IAGOS and DC-8. Most of the overlap is with ATom along the North Atlantic flight corridor in all seasons, ARCTAS over the Canadian Arctic and Greenland in March-May (MAM) and June-August (JJA), and SEAC⁴RS over the Southeast US in September-November (SON). IAGOS NO_y exhibits similar peaks in spring (563 pptv) and summer (565 pptv), due to intensive seasonal lightning in the
250 northern hemisphere (Stratmann et al., 2016). Decline in this source decreases NO_y in autumn to 365 pptv and NO_y further decreases in winter to an annual minimum of 284 pptv.

DC-8 NO_y seasonality is similar to that of IAGOS, though the magnitude of DC-8 NO_y is consistently on average
~130 pptv (range of 80 pptv in SON to 170 pptv in DJF) less than IAGOS NO_y in all seasons. The ~130 pptv
255 greater IAGOS NO_y likely results mostly from differences in sampling altitudes. The two campaigns sample distinct altitude ranges of the upper portion of the upper troposphere centred at ~240 hPa (~10 km) for IAGOS and a wider vertical extent of the lower portion of the upper troposphere centred at ~360 hPa (~1.5 km below IAGOS) for DC-8 (Figure S1). There is a general pattern of a steep increase in NO_y with altitude, with the exception of IAGOS layers located near 300 hPa in March-May and September-November (Figure S1). Average
260 NO_y is similar between the two campaigns for the rare instances that DC-8 and IAGOS sample the same pressure layers (Figure S1). Another minor factor may be IAGOS NO_y instrument interference from HCN. The IAGOS chemiluminescence instruments use a hydrogen (H_2) reagent to convert oxygenated nitrogen compounds to NO , whereas DC-8 uses CO , a compound not permitted on commercial aircraft (Bradshaw et al., 1998; Volz-Thomas et al., 2005; Thomas et al., 2015). The H_2 reagent converts anywhere from 2 to 20% of HCN to NO_y (Weinheimer, 2006). HCN ambient concentrations typically seasonally vary from ~200 to 300 pptv in the upper troposphere,
265 amounting to an interference of 4-60 pptv (Li et al., 2003; Le Breton et al., 2013).

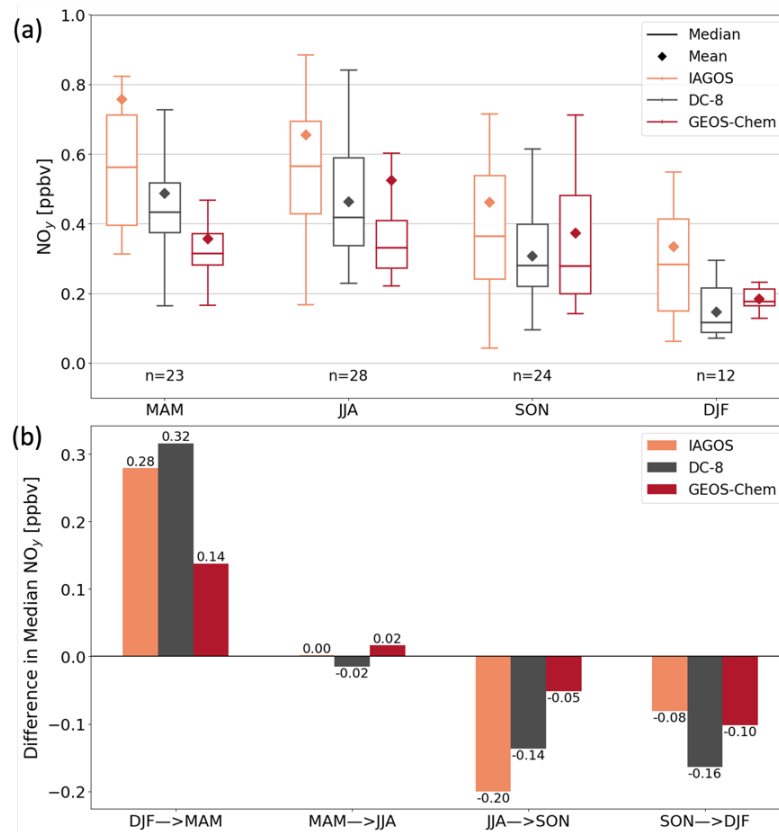


Figure 3: Seasonality of northern hemisphere upper tropospheric NO_y . Panels show seasonal means and medians (a) and seasonal transitions (b) of collocated gridded $2^\circ \times 2.5^\circ$ NO_y from IAGOS (orange), DC-8 (grey), and GEOS-Chem (red). Data in (a) are medians (lines), 25th and 75th percentiles (boxes) and means (diamonds). Inset text in (a) gives the number (n) of overlapping grid cells. Seasonality in (b) is the change in median NO_y in (a) from one season to the next.

Figure 4 shows the relationship between the sum of individual NO_y components and total NO_y for each DC-8 campaign. We use these scatterplots to determine whether most NO_y components are measured in each campaign, given our intention to use DC-8 to assess contemporary understanding of upper tropospheric NO_y . The instruments and individual components of NO_y summed to compare to total NO_y are listed in Table 1. The measured components include NO ; PSS NO_2 (Equation (1)); HNO_3 ; PAN measured as PAN for all ATom sub-campaigns and as part of total PNs for ARCTAS, SEAC⁴RS and KORUS-AQ; HNO_4 measured as HNO_4 for ATom-1 and -2 and as part of total PNs for ARCTAS, SEAC⁴RS and KORUS-AQ; C1-C5 ALKNs for all AToms; total ALKNs for SEAC⁴RS, KORUS-AQ, and ARCTAS; PPN and other PANs for all except ATom-1 and -2; and MPN as part of total PNs for ARCTAS, SEAC⁴RS and KORUS-AQ. The evaluation in Figure 4 is biased toward the northern hemisphere, as the low time resolution sampling of the WAS C1-C5 ALKNs during ATom leads to loss of data in the southern hemisphere (Figure 2) to achieve coincidence of DC-8 total and individual components of NO_y .

Table 1. Observations of individual NO_y components summed to assess budget closure in Figure 4

Component	NASA DC-8 aircraft campaign		
	ARCTAS, SEAC ⁴ RS, KORUS-AQ	ATom1-2	ATom3-4
NO ₂	PSS	PSS	PSS
NO	Chemiluminescence (CL)	CL	CL
HNO ₃	CIMS	CIMS	CIMS
HNO ₄	TD-LIF PNs	CIMS	–
PAN	TD-LIF PNs	PANTHER	PANTHER
PPN	TD-LIF PNs	–	CIMS
other PANs	TD-LIF PNs	–	CIMS
ALKNs	TD-LIF ALKNs	WAS C1-C5	WAS C1-C5
MPN	TD-LIF PNs	–	–

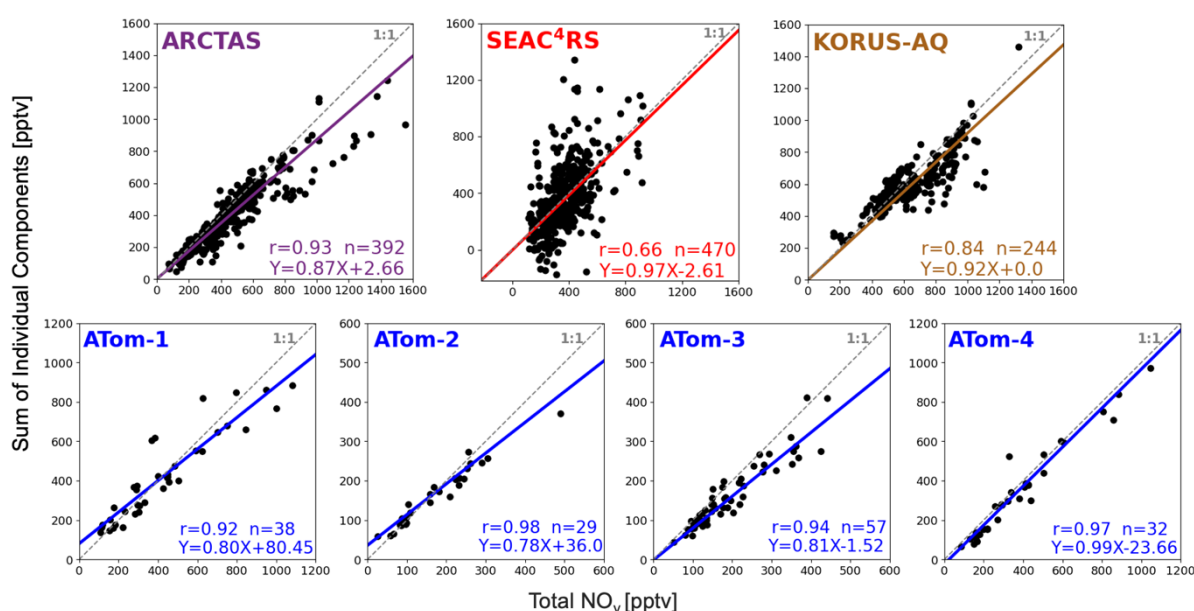


Figure 4: Proportion of reactive oxidized nitrogen components measured during each campaign. Individual points compare the coincident sum of individual NO_y components (Table 1) to measured total NO_y during NASA DC-8 campaigns. Individual NO_y components used in the figure are detailed in the text. Dashed grey lines are the 1:1 relationship. Coloured lines and inset equations are the Theil-Sen regression fit to the observations. Other inset values are the Pearson's correlation coefficient (r) and number of points (n). Axis ranges differ in each panel.

Total measured NO_y and the sum of individual NO_y components are strongly correlated ($r > 0.8$) for all campaigns, except SEAC⁴RS ($r = 0.66$). The weaker correlation for SEAC⁴RS is from the large contribution of MPN to total PNs measured by the TD-LIF instrument. If instead we replace TD-LIF PNs with the sum of CIMS PANs and HNO₄, the correlation with total measured NO_y increases to $r = 0.91$, but the regression slope decreases from 0.97 in Figure 4 to 0.82, as MPN is ~20% of SEAC⁴RS NO_y. The large contribution of MPN to total NO_y during SEAC⁴RS is from aged air initially influenced by lightning, biomass burning and deep convective uplift of surface pollution with large amounts of VOCs and NO_x. These large amounts of VOCs and NO_x cause very active photochemistry that enhances abundance of the MPN precursor, CH₃O₂ (Browne et al., 2011; Nault et al., 2015).

The regression slopes in Figure 4 indicate that most NO_y components are measured during each campaign, ranging from 0.78 for ATom-2 (78% of individual NO_y components measured) to 0.99 for ATom-4 (99% measured). The slopes suggest that between 1-22% of NO_y originates from factors such as unmeasured components, positive interference in the NO_y instrument, or low bias in the TD-LIF PNs. Bradshaw et al. (1998) estimated a temperature-dependent interference from HCN of 8-15% for chemiluminescence instruments that, like those deployed on DC-8 campaigns, use a CO reagent. We estimate a lower-end (8%) interference for mean ambient upper troposphere temperatures measured along the flight paths in Figure 2. Using DC-8 HCN observations, this amounts to ~53 ppt or 12% of NO_y for ARCTAS, ~19 pptv or 5% of NO_y for SEAC⁴RS, ~40 pptv or 6% NO_y for KORUS-AQ, and ~17 pptv or 6% NO_y for ATom 1-4. These lower-end interference estimates are similar in size to the percent unaccounted NO_y (13% for ARCTAS, 3% for SEAC⁴RS, 8% for KORUS-AQ, 1-22% for ATom).

Chemiluminescence NO_y instruments also measure pNO₃, but with uncertain sampling efficiencies (Bourgeois et al., 2022). For 100% sampling efficiency and using the Aerosol Mass Spectrometer (AMS) measurements of submicron (< 1 μm) pNO₃, we estimate a pNO₃ contribution that is at most 1% of NO_y for ARCTAS for a median pNO₃ of ~0.01 μg m⁻³ (~4 pptv), ~4% for SEAC⁴RS for pNO₃ of ~0.04 μg m⁻³ (~14 pptv), ~4% for KORUS-AQ for pNO₃ ~0.07 μg m⁻³ (~25 pptv), and <2% for ATom for pNO₃ <0.01 μg m⁻³ (~4 pptv).

TD-LIF measurements of PNs are calculated from the difference in NO₂ detected with the NO₂ channel and with the PNs channel set to a temperature at which all PNs decompose (Day et al., 2002). A bias in NO₂ could therefore impart a bias in PNs. The largest source of TD-LIF interference is 100% thermal decomposition of MPN (Reed et al., 2016b) and MPN during SEAC⁴RS far exceeds any of the other campaigns. If we use the higher-end MPN interference of 21% from Shah et al. (2023) for SEAC⁴RS, this equates to ~5 pptv of SEAC⁴RS PSS NO₂. This is only ~3% of the 190 pptv SEAC⁴RS PNs.

3.2 Upper tropospheric NO_y composition

Figure 5 provides a breakdown of the absolute and relative contributions of individual NO_y components to total NO_y. ATom-1 and -4 are combined, as these sub-campaigns have a very similar range in NO_y (Figure 4) and in median total and individual components of NO_y, as the sampled seasons (spring and summer) have very similar NO_y (Figure 3). Similarly, ATom-2 and -3 (autumn and winter) are combined. Campaigns are further grouped into remote (ARCTAS, ATom) and continental (SEAC⁴RS, KORUS-AQ), as local influence from continental sources like anthropogenic emissions and intense lightning leads to a greater relative contribution of NO_x and lesser contribution of PAN for the continental upper troposphere and vice versa for the remote upper troposphere.

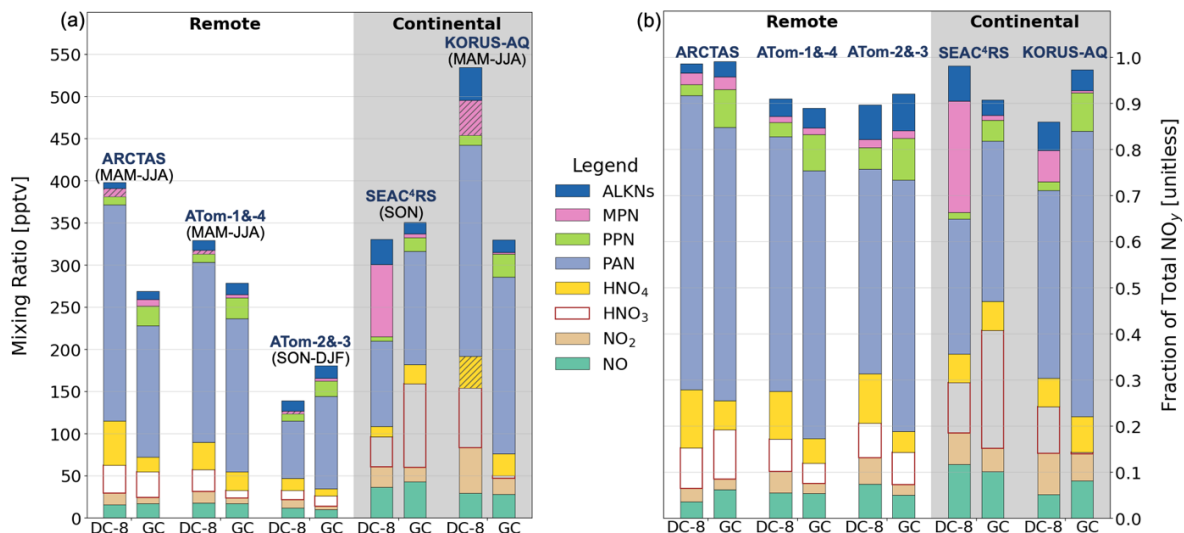


Figure 5: NO_y composition in the upper troposphere along DC-8 flight tracks. Bars are median values of absolute (a) and relative (b) individual NO_y components observed and inferred from the observations during DC-8 campaigns and simulated by GEOS-Chem (GC). Seasons sampled are given above each bar (a) and the grey shading distinguishes sampling in the remote (no shading) and continental (shaded) upper troposphere. Hatchings in (a) indicate inferred concentrations (see text for details). Bar components from bottom to top are NO, NO₂, HNO₃, HNO₄, PAN, PPN, MPN, and ALKNs.

Inferred DC-8 HNO₄ and PPN in Figure 5 use ATom-1 HNO₄ and ATom-4 PPN for combined ATom-1 and -4 components, and, similarly, ATom-2 HNO₄ and ATom-3 PPN for combined ATom-2 and -3. KORUS-AQ HNO₄ is estimated to be 37 pptv by multiplying the SEAC⁴RS median fraction of HNO₄ (HNO₄/NO_y = 0.06) by the KORUS-AQ median NO_y. SEAC⁴RS is used, as HNO₄ is thermally unstable (Ryerson et al., 2000) and so varies with temperature. Mean upper troposphere ambient temperatures for KORUS-AQ (252 K) are more consistent with SEAC⁴RS (246 K) than the other campaigns (238 K for ARCTAS, 238K-241 K for ATom).

The inferred ~10 pptv ARCTAS MPN is from the estimate by Browne et al. (2011). KORUS-AQ MPN is estimated by bounding a potential range from two approaches. The first is the median value of the difference between TD-LIF total PNs and the sum of all individual CIMS PANs and our inferred HNO₄ of 37 pptv, yielding MPN = 75 pptv. This likely overestimates MPN, as the CIMS instrument does not measure an exhaustive suite of PANs. Lee et al. (2022) estimated with a box model and KORUS-AQ measurements that unmeasured PANs account for ~20% of total PNs during KORUS-AQ, though this is for air masses impacted by petrochemical and other anthropogenic VOCs and NO_x emissions. Accounting for these unmeasured PANs yields a lower-bound KORUS-AQ MPN of 8 pptv. The MPN that we infer then for KORUS-AQ is 42 pptv, the midpoint of 8 and 75 pptv, accounting for 7% of KORUS-AQ NO_y. As the GEOS-Chem model MPN is consistent with DC-8 inferred MPN during ARCTAS, we multiply the GEOS-Chem ATom MPN fractions (MPN/NO_y ~0.01 for ATom-1 and -4 and ~0.02 for ATom-2 and -3) by ATom DC-8 NO_y to infer ATom MPN of < 6 pptv.

Only the C1-C5 ALKNs are shown in Figure 5 for ATom. The remote measurements of total ALKNs available from ARCTAS that would be most suitable to assess the likely contribution of longer chain (>C5) ALKNs are on median 5 pptv less than the ATom C1-C5 ALKNs measurements. The ARCTAS total ALKNs measurements are also very noisy, as indicated by a range of -113 pptv to ~333 pptv. The range in ARCTAS WAS C1-C5

375 measurements, by comparison, is 8-29 pptv. Contributions of >C5 ALKNs to total ALKNs for SEAC⁴RS (~50%)
and KORUS-AQ (~60%), representative of the continental upper troposphere, suggest that >C5 ALKNs in remote
regions are <50% of total ALKNs or <12 pptv (median of C1-C5 ALKNs for ATom1-4). According to the
measurements, remote region C1-C5 ALKNs are dominated by methyl nitrate (C1 ALKN), accounting for 40%
of ATom C1-C5 ALKNs and 49% for ARCTAS. Second is isopropyl nitrate (C3 ALKN), making up 17% of
380 ATom C1-C5 ALKNs and 25% for ARCTAS. The >C3 ALKNs dominate ALKNs in the continental upper
troposphere, accounting for 92% of total ALKNs for SEAC⁴RS and 71% for KORUS-AQ. These we estimate as
the difference between TD-LIF total ALKNs and the sum of WAS C1-C3 ALKNs.

The sum of KORUS-AQ NO_y components total 531 pptv, >130 pptv more than SEAC⁴RS, ARCTAS, and ATom-
385 1 and -4 that are within a narrow range of 330-400 pptv. Minimum NO_y are for the remote autumn and winter
measurements from ATom-2 and -3 at 141 pptv. Despite the wide range in absolute total and components of NO_y,
the relative contribution of many individual NO_y components is consistent across all campaigns. These include
NO (7 ± 3%; mean ± 1σ standard deviation), NO₂ (6 ± 2%), HNO₃ (9 ± 2%), HNO₄ (9 ± 3%), PPN (3 ± 1%), and
ALKNs (5 ± 3%). PAN, the dominant NO_y component in all campaigns, is least consistent, ranging from 30-41%
390 for the continental upper troposphere to 44-64% for the remote upper troposphere. The HNO₄ fraction (10-13%)
in the remote upper troposphere is more than the continental upper troposphere (~6%), due to colder temperatures
for ATom and ARCTAS. MPN is uniquely prominent during SEAC⁴RS, accounting for 24% of NO_y compared
to 2-7% inferred for all other campaigns. pNO₃, absent in Figure 5 due to the uncertain sampling efficiency of the
chemiluminescence instrument, is at most 4% for SEAC⁴RS and KORUS-AQ (Section 3.1), comparable to the
395 contribution from PPN.

The far larger fraction of MPN to total NO_y during SEAC⁴RS (Figure 5(b)) warrants further investigation. If we
instead estimate MPN by subtracting the sum of HNO₄ and all PANs measured with the CIMS instrument from
the TD-LIF PNs, making the assumption that CIMS measures most PANs, MPN is 49 pptv and the contribution
400 to NO_y declines from 24% to 14%. This is still at least double the contribution for any other campaign.

The NO_y composition information in Figure 5 has a northern hemisphere sampling bias to achieve coincidence.
ATom observations south of the Equator exhibit a similar seasonal pattern to the northern hemisphere: summer >
spring > autumn > winter NO_y, except that the southern hemisphere spring and summer NO_y differ by ~90 pptv,
405 whereas there is near-negligible difference for the northern hemisphere (Figure 3). As with the northern
hemisphere, PAN accounts for most southern hemisphere NO_y, ranging from ~32% for ATom-1 (July-August) to
~42% for ATom-2 (January-February).

Nighttime dominant NO_y compounds N₂O₅, NO₃, and HONO are not included in Figure 5, as these have near-
410 negligible daytime abundances. Of these, there are only measurements of N₂O₅, limited to ATom-3 and -4, that
represent ~0.1% of upper tropospheric NO_y along the daytime ATom flight tracks in Figure 2. NO₃ has a lifetime
of a few seconds during the day, due to efficient photolysis (Brown and Stutz, 2012). HONO also rapidly
photolyzes with a near-surface lifetime of 15 min (Sörgel et al., 2011). Photolysis of HONO would be further

enhanced (by ~50% at 390 nm) in the upper troposphere where photolysis frequencies are enhanced (Hofzumahaus et al., 2002; Reed et al., 2016a).

3.3 Contemporary understanding of UT NO_y

GEOS-Chem northern hemisphere upper troposphere NO_y is compared to the observations in Figures 3 and 5. In Figure 3, GEOS-Chem median NO_y is less than DC-8 in summer and spring by ~103 pptv, similar to DC-8 in autumn, and greater than DC-8 in winter by ~60 pptv. As a result of these differences in absolute NO_y, the model underestimates the IAGOS and DC-8 seasonal shifts in NO_y from winter to spring and from summer to autumn.

The sum of the GEOS-Chem fractional contributions of NO_y components in Figure 5(b) that do not sum to 1 are because the model NO_y budget also includes components not measured during DC-8, such as MPAN and halogenated ALKNs. Consistent across all campaigns is model underestimate in NO₂ and overestimate in PPN. The model version we use does not include photolysis of PPN, even though this is known to occur (Harwood et al., 2003). PPN photolysis rather than thermal decomposition is the dominant loss pathway of PPN in the cold upper troposphere. PPN photolysis is scheduled for inclusion in a later model version (version 14.5) than is used here (Horner et al., 2024). Inclusion of PPN photolysis would liberate up to ~16 pptv NO₂, resolving the 10-16 pptv model underestimate in NO₂. Other studies have addressed model biases in NO₂ by including photolysis of pNO₃ forming HONO that rapidly photolyses to NO_x (Shah et al., 2023; Horner et al., 2024). pNO₃ concentrations are too small in the upper troposphere for this to be a substantial NO₂ source. These are on median, ~0.01 µg m⁻³ during ARCTAS, ~0.07 µg m⁻³ during KORUS-AQ, ~0.04 µg m⁻³ during SEAC⁴RS and <0.01 µg m⁻³ during ATom (Section 3.1).

The model exhibits significant campaign-specific biases in total NO_y for ARCTAS (129 pptv underestimate), KORUS-AQ (205 pptv underestimate), ATom-1 and -4 (51 pptv underestimate) and ATom-2 and -3 (42 pptv overestimate). The model underestimate in ARCTAS NO_y is due mostly to a ~100 pptv low bias in PAN and, to a lesser extent, a 35 pptv underestimate in HNO₄. The model bias for ATom-2 and -3 is due almost entirely to PAN. For KORUS-AQ, all NO_y components except PPN are underestimated, indicative of an overall underestimate in NO_y sources to the upper troposphere over this region. The ATom-1 and -4 underestimate in NO_y is due mostly to a low model bias in PAN and HNO₃. Overall, the model underestimates the contrast in upper tropospheric NO_y between the remote and continental upper troposphere.

GEOS-Chem simulates individual C1-C3 ALKNs, but most >C3 ALKNs are included as a lumped species. There are other >C3 ALKNs represented individually in the model, such as those formed from isoprene oxidation (Fisher et al., 2016), but abundances of these are near-negligible in the upper troposphere. DC-8 C1 ALKN is only 4% of ALKNs for SEAC⁴RS and 11% for KORUS-AQ, whereas in the model these are a much greater component of ALKNs: 40% for SEAC⁴RS and 29% for KORUS-AQ. Modelled >C3 ALKNs are a far smaller portion of total ALKNs (29% for SEAC⁴RS and 23% for KORUS-AQ) than the observations (Sect. 3.2). Modelled C1 ALKN concentrations are consistently less than the observed values by ~2 pptv for ARCTAS and ~1 pptv for ATom.

Modelled C3 ALKN is ~1 pptv less than the observations for ARCTAS, but ~1 pptv more than the observations for ATom.

The sum of measured and modelled individual NO_y components are not significantly different for SEAC⁴RS, though the model overestimates HNO_3 by 64 pptv and underestimates MPN by 81 pptv compared to the TD-LIF measurements and by 45 pptv compared to MPN inferred using TD-LIF PNs and CIMS HNO_4 and PANs (Section 3.2). The model low bias in MPN suggests that the model underestimates influence of NO_x and reactive VOCs sources on aged air over source regions with a mix of emissions from fires and lightning, and deep convective injection of surface pollution. Chen et al. (2019) estimated that the GEOS-Chem underestimate in free tropospheric VOCs during SEAC⁴RS is on average ~60%, but exceeds a factor of 2 for many of the VOCs assessed. The model high bias in HNO_3 could be because of a factor of 2 overestimate in our modelled H_2O_2 compared to observed H_2O_2 for SEAC⁴RS. An overestimate in H_2O_2 indicates a model overestimate in HO_2 that promotes formation of HNO_3 and that would also account for the ~10 pptv overestimate in modelled HNO_4 . Modelled HO_2 is used to calculate PSS NO_2 for SEAC⁴RS (Equation (1), Sect. 2.1), but this only imparts a small high bias (~1.7 pptv) in SEAC⁴RS PSS NO_2 . Model bias in H_2O_2 for ARCTAS (>100 pptv) may also be the cause for the model underestimate in ARCTAS HNO_4 of ~35 pptv.

Modelled KORUS-AQ HNO_3 , ALKNs, and MPN are all biased low. The low biases in these NO_y components may be because of a general underestimate in NO_y sources over South Korea where there are large anthropogenic NO_x and VOCs sources that are represented in the model with a global inventory (CEDs) that may not suitably account for local emissions (Travis et al., 2024). Lightning NO_x emissions could also be underestimated in the heavily parameterized inventory in GEOS-Chem (Murray et al., 2012; Marais et al., 2018), but this is a challenging NO_x source to evaluate over locations that include other prominent sources of NO_x .

The model biases identified in this work hinder accurate determination of the radiative effect of tropospheric ozone for short-term climate impact assessments, the oxidative capacity of the troposphere for quantifying the lifetime and persistence of the greenhouse gas methane, tropospheric column densities of NO_2 from space-based UV-visible instruments that are retrieved with modelled vertical profiles of NO_2 , NO_x emissions by comparing modelled and observed oxidized nitrate wet deposition fluxes that depend on the abundance of soluble HNO_3 , and harm of nitrogen deposition to vulnerable habitats.

4 Conclusions

We used NASA DC-8 aircraft measurement data from the ARCTAS, SEAC⁴RS, KORUS-AQ, and ATom campaigns to characterize reactive oxidized nitrogen (NO_y) in the global upper troposphere. This followed confirmation from comparison to routine total NO_y measurements from the IAGOS commercial aircraft campaign that DC-8 has the same seasonality of peak NO_y in summer and spring and minimum NO_y in winter in the northern hemisphere. Consistency supports use of DC-8 campaign data to characterise NO_y under standard daytime conditions.

We also confirm that most (78-99%) NO_y components were measured during DC-8 campaigns. These include nitrogen oxides (NO_x), and inorganic (HNO_3 and HNO_4), and organic (PANs, MPN, and alkyl nitrates) reservoirs of NO_x . PAN is the dominant NO_y component for all campaigns (30-64%), followed by NO_x (6-18%), HNO_4 (6-13%) and HNO_3 (7-11%). The relative contribution of most other components is similar across all campaigns, except for MPN that is 15-24% of NO_y for SEAC⁴RS over the Southeast US and much less (2-7%) for all other campaigns, though MPN measurements are rare and susceptible to biases.

The GEOS-Chem model is sampled along the DC-8 flight tracks to assess the state of knowledge of upper tropospheric NO_y . Consistent model biases for all campaigns include an overestimate in PPN and underestimate in NO_2 . The model lacks PPN photolysis that would address the PPN model bias and mostly resolve the NO_2 bias. In the continental upper troposphere, the model underestimates total NO_y for KORUS-AQ, but reproduces total NO_y for SEAC⁴RS, though with too much HNO_3 and too little MPN. Over remote regions, the model biases are less severe, and are likely related to the weak seasonal variability in total NO_y in comparison to DC-8 and IAGOS. A possible cause of this is errors in model representation of maritime lightning NO_x emissions that influence NO_y abundance in spring and summer.

Our results underscore the need for sustained measurements of upper tropospheric reactive oxidized nitrogen for further refinement of knowledge of upper tropospheric NO_y sources, advection, and chemical processing. This is crucial for advancing our understanding of the global nitrogen cycle and its broader environmental impacts.

Author Contributions

Study concept by EAM and NW. NW led the data analysis and simulated GEOS-Chem. The manuscript is initiated by NW and co-written by EAM. GL aided in data analysis, RGR in the use of ObsPack, and BS in the use of IAGOS NO_y observations. All authors reviewed and edited the manuscript.

Competing interests

The authors declare that they have no conflict of interest.

Acknowledgements

We are grateful for the provision of the NASA DC-8 aircraft observations by the instrument PIs Paul O. Wennberg, Ronald C. Cohen, Thomas B. Ryerson, Chelsea Thompson, Andrew Weinheimer, L. Gregory Huey, Jim Elkins, and Donald R. Blake and, for IAGOS, the IAGOS-Core data provided by Andreas Volz-Thomas and IAGOS-CARABIC by Helmut Ziereis. The authors acknowledge the strong support of the European Commission, Airbus, and the airlines (Lufthansa, Air France, Austrian Airlines, Air Namibia, Cathay Pacific, Iberia and China Airlines so far) who have carried the IAGOS-Core equipment and performed the maintenance since 1994. IAGOS-CARABIC NO_y measurement funding is from the German Aerospace Centre (DLR). In its last 10 years of operation, IAGOS-Core has been funded by INSU-CNRS (France), Météo-France, Université Paul Sabatier (Toulouse, France) and Forschungszentrum Jülich (FZJ, Jülich, Germany). IAGOS has been additionally funded by the EU projects IAGOSDS and IAGOS-ERI. The IAGOS-Core and the IAGOS-CARABIC database are

supported by AERIS. IAGOS-CARIBIC data are also available from the IAGOS-CARIBIC team (see <http://www.caribic-atmospheric.com>)

535 Data and Software Availability

All data and software used in this study are from publicly accessible repositories: Zenodo for GEOS-Chem (The International GEOS-Chem User Community, 2021), the AERIS data service for IAGOS (Boulanger et al., 2018), and NASA data archives for ARCTAS (NASA, 2009), SEAC⁴RS (NASA, 2015), KORUS-AQ (NASA, 2017), and ATom (NASA, 2021).

540

Funding

This research has been supported by the European Research Council under the European Union's Horizon 2020 research and innovation programme (through a Starting Grant awarded to Eloise A. Marais, UpTrop [grant no. 851854]).

545

References

Amos, H. M., Jacob, D. J., Holmes, C., Fisher, J. A., Wang, Q., Yantosca, R. M., Corbitt, E. S., Galarneau, E., Rutter, A., and Gustin, M.: Gas-particle partitioning of atmospheric Hg (II) and its effect on global mercury deposition, *Atmos. Chem. Phys.*, 12, 591-603, doi:10.5194/acp-12-591-2012, 2012.

550 Barth, M. C., Cantrell, C. A., Brune, W. H., Rutledge, S. A., Crawford, J. H., Huntrieser, H., Carey, L. D., MacGorman, D., Weisman, M., Pickering, K. E., et al.: The Deep Convective Clouds and Chemistry (DC3) Field Campaign, *B. Am. Meteorol. Soc.*, 96, 1281-1309, doi:10.1175/bams-d-13-00290.1, 2015.

Bertram, T. H., Perring, A. E., Wooldridge, P. J., Crounse, J. D., Kwan, A. J., Wennberg, P. O., Scheuer, E., Dibb, J., Avery, M., Sachse, G., et al.: Direct measurements of the convective recycling of the upper
555 troposphere, *Science*, 315, 816-820, doi:10.1126/science.1134548, 2007.

Blake, N. J., Blake, D. R., Swanson, A. L., Atlas, E., Flocke, F., and Rowland, F. S.: Latitudinal, vertical, and seasonal variations of C1-C4 alkyl nitrates in the troposphere over the Pacific Ocean during PEM-Tropics A and B: Oceanic and continental sources, *J. Geophys. Res.-Atmos.*, 108, doi:10.1029/2001JD001444, 2003.

Blakeslee, R. J., Mach, D. M., Bateman, M. G., and Bailey, J. C.: Seasonal variations in the lightning diurnal cycle and implications for the global electric circuit, *Atmos. Res.*, 135-136, 228-243, doi:10.1016/j.atmosres.2012.09.023, 2014.

Boersma, K. F., Eskes, H. J., Dirksen, R. J., van der A, R. J., Veefkind, J. P., Stammes, P., Huijnen, V., Kleipool, Q. L., Sneep, M., Claas, J., et al.: An improved tropospheric NO₂ column retrieval algorithm for the Ozone Monitoring Instrument, *Atmos. Meas. Tech.*, 4, 1905-1928, doi:10.5194/amt-4-1905-2011, 2011.

565 Boulanger, D., Blot, R., Bundke, U., Gerbig, C., Hermann, M., Nédélec, P., Rohs, S., and Ziereis, H., IAGOS final quality controlled Observational Data L2 – Vertical profiles. [dataset]. AERIS, [last accessed: 3 September 2021], 2018.

Bourgeois, I., Peischl, J., Neuman, J. A., Brown, S. S., Allen, H. M., Campuzano-Jost, P., Coggon, M. M., DiGangi, J. P., Diskin, G. S., Gilman, J. B., et al.: Comparison of airborne measurements of NO, NO₂, HONO, NO_y, and CO during FIREX-AQ, *Atmos. Meas. Tech.*, 15, 4901-4930, doi:10.5194/amt-15-4901-2022, 2022.

570

- Bradshaw, J., Sandholm, S., and Talbot, R.: An update on reactive odd-nitrogen measurements made during recent NASA Global Tropospheric Experiment programs, *J. Geophys. Res.-Atmos.*, 103, 19129-19148, doi:10.1029/98JD00621, 1998.
- 575 Bradshaw, J., Davis, D., Grodzinsky, G., Smyth, S., Newell, R., Sandholm, S., and Liu, S.: Observed distributions of nitrogen oxides in the remote free troposphere from the NASA Global Tropospheric Experiment Programs, *Rev. Geophys.*, 38, 61-116, doi:10.1029/1999rg900015, 2000.
- Brasseur, G. P., Müller, J.-F., and Granier, C.: Atmospheric impact of NO_x emissions by subsonic aircraft: A three dimensional model study, *J. Geophys. Res.-Atmos.*, 101, 1423-1428, doi:10.1029/95jd02363, 1996.
- 580 Brenninkmeijer, C. A. M., Crutzen, P., Boumard, F., Dauer, T., Dix, B., Ebinghaus, R., Filippi, D., Fischer, H., Franke, H., Frieß, U., et al.: Civil aircraft for the regular investigation of the atmosphere based on an instrumented container: The new CARIBIC system, *Atmos. Chem. Phys.*, 7, 4953-4976, doi:10.5194/acp-7-4953-2007, 2007.
- Brown, S. S., and Stutz, J.: Nighttime radical observations and chemistry, *Chem. Soc. Rev.*, 41, 6405-6447, doi:10.1039/C2CS35181A, 2012.
- 585 Browne, E. C., Perring, A. E., Wooldridge, P. J., Apel, E., Hall, S. R., Huey, L. G., Mao, J., Spencer, K. M., Clair, J. M. S., Weinheimer, A. J., et al.: Global and regional effects of the photochemistry of CH₃O₂NO₂: Evidence from ARCTAS, *Atmos. Chem. Phys.*, 11, 4209-4219, doi:10.5194/acp-11-4209-2011, 2011.
- 590 Burkholder, J. B., Sander, S. P., Abbatt, J., Barker, J. R., Cappa, C., Crounse, J. D., Dibble, T. S., Huie, R. E., Kolb, C. E., Kurylo, M. J., Orkin, V. L., Percival, C. J., Wilmouth, D. M., and Wine, P. H.: Chemical kinetics and photochemical data for use in atmospheric studies, evaluation No. 19, JPL Publication 19-5, 2020.
- Chen, X., Millet, D. B., Singh, H. B., Wisthaler, A., Apel, E. C., Atlas, E. L., Blake, D. R., Bourgeois, I., Brown, S. S., Crounse, J. D., et al.: On the sources and sinks of atmospheric VOCs: An integrated analysis of recent aircraft campaigns over North America, *Atmos. Chem. Phys.*, 19, 9097-9123, doi:10.5194/acp-19-9097-2019, 2019.
- 595 Cohen, Y., Hauglustaine, D., Sauvage, B., Rohs, S., Konjari, P., Bundke, U., Petzold, A., Thouret, V., Zahn, A., and Ziereis, H.: Evaluation of modelled climatologies of O₃, CO, water vapour and NO_y in the upper troposphere–lower stratosphere using regular in situ observations by passenger aircraft, *Atmos. Chem. Phys.*, 23, 14973-15009, doi:10.5194/acp-23-14973-2023, 2023.
- 600 Crawford, J. H., Ahn, J.-Y., Al-Saadi, J., Chang, L., Emmons, L. K., Kim, J., Lee, G., Park, J.-H., Park, R. J., Woo, J. H., et al.: The Korea–United States Air Quality (KORUS-AQ) field study, *Elementa: Science of the Anthropocene*, 9, doi:10.1525/elementa.2020.00163, 2021.
- Crounse, J. D., McKinney, K. A., Kwan, A. J., and Wennberg, P. O.: Measurement of gas-phase hydroperoxides by Chemical Ionization Mass Spectrometry, *Anal. Chem.*, 78, 6726-6732, doi:10.1021/ac0604235, 2006.
- 605 Culter, F., NASA DC-8 Flying Laboratory Aircraft, https://ghrc.nsstc.nasa.gov/home/sites/default/files/cutler_dc8.pdf, [last accessed: 3 October 2024], 2009.
- Dahlmann, K., Grewe, V., Ponater, M., and Matthes, S.: Quantifying the contributions of individual NO_x sources to the trend in ozone radiative forcing, *Atmos. Environ.*, 45, 2860-2868, doi:10.1016/j.atmosenv.2011.02.071, 2011.

- 610 Dameris, M.: Stratosphere/Troposphere exchange and structure | Tropopause, in: Encyclopedia of Atmospheric Sciences (Second Edition), edited by: North, G. R., Pyle, J., and Zhang, F., Academic Press, Oxford, 269-272, doi:<https://doi.org/10.1016/B978-0-12-382225-3.00418-7>, 2015.
- Day, D. A., Wooldridge, P. J., Dillon, M. B., Thornton, J. A., and Cohen, R. C.: A thermal dissociation laser-induced fluorescence instrument for in situ detection of NO₂, peroxy nitrates, alkyl nitrates, and HNO₃, J. Geophys. Res.: Atmos., 107, doi:10.1029/2001jd000779, 2002.
- 615 Ehhalt, D. H., Rohrer, F., and Wahner, A.: Sources and distribution of NO_x in the upper troposphere at northern mid-latitudes, J. Geophys. Res.-Atmos., 97, 3725-3738, doi:10.1029/91JD03081, 1992.
- Emmons, L. K., Carroll, M. A., Hauglustaine, D. A., Brasseur, G. P., Atherton, C., Penner, J., Sillman, S., Levy, H., Rohrer, F., Wauben, W. M. F., et al.: Climatologies of NO_x and NO_y: A comparison of data and models, Atmos. Environ., 31, 1851-1904, doi:10.1016/s1352-2310(96)00334-2, 1997.
- 620 Fisher, J. A., Jacob, D. J., Travis, K. R., Kim, P. S., Marais, E. A., Chan Miller, C., Yu, K., Zhu, L., Yantosca, R. M., Sulprizio, M. P., et al.: Organic nitrate chemistry and its implications for nitrogen budgets in an isoprene- and monoterpene-rich atmosphere: constraints from aircraft (SEAC⁴RS) and ground-based (SOAS) observations in the Southeast US, Atmos. Chem. Phys., 16, 5969-5991, doi:10.5194/acp-16-5969-2016, 2016.
- 625 Fisher, J. A., Atlas, E. L., Barletta, B., Meinardi, S., Blake, D. R., Thompson, C. R., Ryerson, T. B., Peischl, J., Tzompa-Sosa, Z. A., and Murray, L. T.: Methyl, ethyl, and propyl nitrates: Global distribution and impacts on reactive nitrogen in remote marine environments, J. Geophys. Res.-Atmos., 123, doi:10.1029/2018jd029046, 2018.
- 630 Fuelberg, H. E., Hannan, J. R., van Velthoven, P. F. J., Browell, E. V., Bieberbach Jr., G., Knabb, R. D., Gregory, G. L., Pickering, K. E., and Selkirk, H. B.: A meteorological overview of the Subsonic Assessment Ozone and Nitrogen Oxide Experiment (SONEX) period, J. Geophys. Res.-Atmos., 105, 3633-3651, doi:10.1029/1999JD900917, 2000.
- Giglio, L., Randerson, J. T., and van der Werf, G. R.: Analysis of daily, monthly, and annual burned area using the fourth-generation global fire emissions database (GFED4), J. Geophys. Res.-Biogeo., 118, 317-328, doi:10.1002/jgrg.20042, 2013.
- 635 Gressent, A., Sauvage, B., Defer, E., Pätz, H. W., Thomas, K., Holle, R., Cammas, J.-P., Nédélec, P., Boulanger, D., Thouret, V., et al.: Lightning NO_x influence on large-scale NO_y and O₃ plumes observed over the northern mid-latitudes, Tellus B, 66, doi:10.3402/tellusb.v66.25544, 2014.
- 640 Gressent, A., Sauvage, B., Cariolle, D., Evans, M., Leriche, M., Mari, C., and Thouret, V.: Modeling lightning-NO_x chemistry on a sub-grid scale in a global chemical transport model, Atmos. Chem. Phys., 16, 5867-5889, doi:10.5194/acp-16-5867-2016, 2016.
- Guenther, A. B., Jiang, X., Heald, C. L., Sakulyanontvittaya, T., Duhl, T., Emmons, L. K., and Wang, X.: The Model of Emissions of Gases and Aerosols from Nature version 2.1 (MEGAN2.1): An extended and updated framework for modeling biogenic emissions, Geosci. Model Dev., 5, 1471-1492, doi:10.5194/gmd-5-1471-2012, 2012.
- 645 Harwood, M. H., Roberts, J. M., Frost, G. J., Ravishankara, A. R., and Burkholder, J. B.: Photochemical Studies of CH₃C(O)OONO₂ (PAN) and CH₃CH₂C(O)OONO₂ (PPN): NO₃ Quantum Yields, J. Phys. Chem. A, 107, 1148-1154, doi:10.1021/jp0264230, 2003.
- Hoesly, R. M., Smith, S. J., Feng, L., Klimont, Z., Janssens-Maenhout, G., Pitkanen, T., Seibert, J. J., Vu, L., Andres, R. J., Bolt, R. M., et al.: Historical (1750–2014) anthropogenic emissions of reactive gases and aerosols

- 650 from the Community Emissions Data System (CEDS), *Geosci. Model Dev.*, 11, 369-408, doi:10.5194/gmd-11-369-2018, 2018.
- Hofzumahaus, A., Kraus, A., Kylling, A., and Zerefos, C. S.: Solar actinic radiation (280–420 nm) in the cloud-free troposphere between ground and 12 km altitude: Measurements and model results, *J. Geophys. Res.: Atmos.*, 107, doi:10.1029/2001jd900142, 2002.
- 655 Horner, R. P., Marais, E. A., Wei, N., Ryan, R. G., and Shah, V.: Vertical profiles of global tropospheric nitrogen dioxide (NO₂) obtained by cloud slicing the TROPOspheric Monitoring Instrument (TROPOMI), *Atmos. Chem. Phys.*, 24, 13047-13064, doi:10.5194/acp-24-13047-2024, 2024.
- Hudman, R. C., Jacob, D. J., Turquety, S., Leibensperger, E. M., Murray, L. T., Wu, S., Gilliland, A. B., Avery, M., Bertram, T. H., Brune, W., et al.: Surface and lightning sources of nitrogen oxides over the United States: Magnitudes, chemical evolution, and outflow, *J. Geophys. Res.*, 112, doi:10.1029/2006jd007912, 2007.
- 660 Hudman, R. C., Moore, N. E., Mebust, A. K., Martin, R. V., Russell, A. R., Valin, L. C., and Cohen, R. C.: Steps towards a mechanistic model of global soil nitric oxide emissions: implementation and space based-constraints, *Atmos. Chem. Phys.*, 12, 7779-7795, doi:10.5194/acp-12-7779-2012, 2012.
- Huey, L. G.: Measurement of trace atmospheric species by chemical ionization mass spectrometry: Speciation of reactive nitrogen and future directions, *Mass Spectrom. Rev.*, 26, 166-184, doi:10.1002/mas.20118, 2007.
- 665 Huntrieser, H., Lichtenstern, M., Scheibe, M., Aufmhoff, H., Schlager, H., Pucik, T., Minikin, A., Weinzierl, B., Heimerl, K., Pollack, I. B., et al.: Injection of lightning-produced NO_x, water vapor, wildfire emissions, and stratospheric air to the UT/LS as observed from DC3 measurements, *J. Geophys. Res.-Atmos.*, 121, 6638-6668, doi:10.1002/2015JD024273, 2016.
- 670 Jacob, D. J., Crawford, J. H., Maring, H., Clarke, A. D., Dibb, J. E., Emmons, L. K., Ferrare, R. A., Hostetler, C. A., Russell, P. B., Singh, H. B., et al.: The Arctic Research of the Composition of the Troposphere from Aircraft and Satellites (ARCTAS) mission: Design, execution, and first results, *Atmos. Chem. Phys.*, 10, 5191-5212, doi:10.5194/acp-10-5191-2010, 2010.
- Jaeglé, L., Jacob, D. J., Wang, Y., Weinheimer, A. J., Ridley, B. A., Campos, T. L., Sachse, G. W., and Hagen, D. E.: Sources and chemistry of NO_x in the upper troposphere over the United States, *Geophys. Res. Lett.*, 25, 1705-1708, doi:10.1029/97gl03591, 1998.
- 675 Le Breton, M., Bacak, A., Muller, J. B. A., O'Shea, S. J., Xiao, P., Ashfold, M. N. R., Cooke, M. C., Batt, R., Shallcross, D. E., Oram, D. E., et al.: Airborne hydrogen cyanide measurements using a chemical ionisation mass spectrometer for the plume identification of biomass burning forest fires, *Atmos. Chem. Phys.*, 13, 9217-9232, doi:10.5194/acp-13-9217-2013, 2013.
- 680 Lee, Y. R., Huey, L. G., Tanner, D. J., Takeuchi, M., Qu, H., Liu, X., Ng, N. L., Crawford, J. H., Fried, A., Richter, D., et al.: An investigation of petrochemical emissions during KORUS-AQ: Ozone production, reactive nitrogen evolution, and aerosol production, *Elementa: Science of the Anthropocene*, 10, doi:10.1525/elementa.2022.00079, 2022.
- 685 Levy II, H., Mahlman, J. D., and Moxim, W. J.: A stratospheric source of reactive nitrogen in the unpolluted troposphere, *Geophys. Res. Lett.*, 7, 441-444, doi:10.1029/GL007i006p00441, 1980.
- Levy II, H., Moxim, W. J., Klonecki, A. A., and Kasibhatla, P. S.: Simulated tropospheric NO_x: Its evaluation, global distribution and individual source contributions, *J. Geophys. Res.-Atmos.*, 104, 26279-26306, doi:10.1029/1999JD900442, 1999.

- 690 Li, Q., Jacob, D. J., Yantosca, R. M., Heald, C. L., Singh, H. B., Koike, M., Zhao, Y., Sachse, G. W., and Streets, D. G.: A global three-dimensional model analysis of the atmospheric budgets of HCN and CH₃CN: Constraints from aircraft and ground measurements, *J. Geophys. Res.-Atmos.*, 108, doi:10.1029/2002JD003075, 2003.
- 695 Liang, Q., Rodriguez, J. M., Douglass, A. R., Crawford, J. H., Olson, J. R., Apel, E., Bian, H., Blake, D. R., Brune, W., Chin, M., et al.: Reactive nitrogen, ozone and ozone production in the Arctic troposphere and the impact of stratosphere-troposphere exchange, *Atmos. Chem. Phys.*, 11, 13181-13199, doi:10.5194/acp-11-13181-2011, 2011.
- Logan, J. A.: Nitrogen oxides in the troposphere: Global and regional budgets, *J. Geophys. Res.-Oceans*, 88, 10785-10807, doi:10.1029/JC088iC15p10785, 1983.
- 700 Luo, G., Yu, F., and Moch, J. M.: Further improvement of wet process treatments in GEOS-Chem v12.6.0: Impact on global distributions of aerosols and aerosol precursors, *Geosci. Model Dev.*, 13, 2879-2903, doi:10.5194/gmd-13-2879-2020, 2020.
- 705 Marais, E. A., Jacob, D. J., Choi, S., Joiner, J., Belmonte-Rivas, M., Cohen, R. C., Beirle, S., Murray, L. T., Schiferl, L. D., Shah, V., et al.: Nitrogen oxides in the global upper troposphere: interpreting cloud-sliced NO₂ observations from the OMI satellite instrument, *Atmos. Chem. Phys.*, 18, 17017-17027, doi:10.5194/acp-18-17017-2018, 2018.
- Marais, E. A., Roberts, J. F., Ryan, R. G., Eskes, H., Boersma, K. F., Choi, S., Joiner, J., Abuhassan, N., Redondas, A., Grutter, M., et al.: New observations of NO₂ in the upper troposphere from TROPOMI, *Atmos. Meas. Tech.*, 14, 2389-2408, doi:10.5194/amt-14-2389-2021, 2021.
- 710 Marengo, A., Thouret, V., Nédélec, P., Smit, H., Helten, M., Kley, D., Karcher, F., Simon, P., Law, K., Pyle, J., et al.: Measurement of ozone and water vapor by Airbus in-service aircraft: The MOZAIC airborne program, an overview, *J. Geophys. Res.-Atmos.*, 103, 25631-25642, doi:10.1029/98jd00977, 1998.
- 715 Mickley, L. J., Murti, P. P., Jacob, D. J., Logan, J. A., Koch, D. M., and Rind, D.: Radiative forcing from tropospheric ozone calculated with a unified chemistry-climate model, *J. Geophys. Res.-Atmos.*, 104, 30153-30172, doi:10.1029/1999jd900439, 1999.
- Murray, L. T., Jacob, D. J., Logan, J. A., Hudman, R. C., and Koshak, W. J.: Optimized regional and interannual variability of lightning in a global chemical transport model constrained by LIS/OTD satellite data, *J. Geophys. Res.-Atmos.*, 117, doi:10.1029/2012jd017934, 2012.
- 720 Murray, L. T., Logan, J. A., and Jacob, D. J.: Interannual variability in tropical tropospheric ozone and OH: The role of lightning, *J. Geophys. Res.-Atmos.*, 118, 411,468-411,480, doi:10.1002/jgrd.50857, 2013.
- Murray, L. T., Fiore, A. M., Shindell, D. T., Naik, V., and Horowitz, L. W.: Large uncertainties in global hydroxyl projections tied to fate of reactive nitrogen and carbon, *P. Natl. Acad. Sci. USA*, 118, e2115204118, doi:10.1073/pnas.2115204118, 2021.
- 725 NASA, NASA: Airborne Science Data for Atmospheric Composition: <https://www-air.larc.nasa.gov/cgi-bin/ArcView/arctas?DC8=1>, [last accessed: 24 October], 2009.
- NASA, NASA: Airborne Science Data for Atmospheric Composition: <https://www-air.larc.nasa.gov/cgi-bin/ArcView/seac4rs>, [last accessed: 24 October], 2015.
- NASA, NASA: EARTHDATA, Korea United States Air Quality Study: <https://asdc.larc.nasa.gov/project/KORUS-AQ>, [last accessed: 24 October], 2017.

- 730 NASA, NASA: EARTHDATA, ATom: Merged Atmospheric Chemistry, Trace Gases, and Aerosols, Version 2: https://daac.ornl.gov/cgi-bin/dsviewer.pl?ds_id=1925, [last accessed: 24 October], 2021.
- Nault, B. A., Garland, C., Pusede, S. E., Wooldridge, P. J., Ullmann, K., Hall, S. R., and Cohen, R. C.: Measurements of CH₃O₂NO₂ in the upper troposphere, *Atmos. Meas. Tech.*, 8, 987-997, doi:10.5194/amt-8-987-2015, 2015.
- 735 Petzold, A., Thouret, V., Gerbig, C., Zahn, A., Brenninkmeijer, C. A. M., Gallagher, M., Hermann, M., Pontaud, M., Ziereis, H., Boulanger, D., et al.: Global-scale atmosphere monitoring by in-service aircraft – Current achievements and future prospects of the European Research Infrastructure IAGOS, *Tellus B*, 67, 28452, doi:10.3402/tellusb.v67.28452, 2015.
- 740 Pollack, I. B., Lerner, B. M., and Ryerson, T. B.: Evaluation of ultraviolet light-emitting diodes for detection of atmospheric NO₂ by photolysis - chemiluminescence, *J. Atmos. Chem.*, 65, 111-125, doi:10.1007/s10874-011-9184-3, 2010.
- Prather, M. J., and Jacob, D. J.: A persistent imbalance in HO_x and NO_x photochemistry of the upper troposphere driven by deep tropical convection, *Geophys. Res. Lett.*, 24, 3189-3192, doi:<https://doi.org/10.1029/97GL03027>, 1997.
- 745 Rap, A., Richards, N. A. D., Forster, P. M., Monks, S. A., Arnold, S. R., and Chipperfield, M. P.: Satellite constraint on the tropospheric ozone radiative effect, *Geophys. Res. Lett.*, 42, 5074-5081, doi:10.1002/2015gl064037, 2015.
- 750 Reed, C., Brumby, C. A., Crilley, L. R., Kramer, L. J., Bloss, W. J., Seakins, P. W., Lee, J. D., and Carpenter, L. J.: HONO measurement by differential photolysis, *Atmos. Meas. Techn.*, 9, 2483-2495, doi:10.5194/amt-9-2483-2016, 2016a.
- Reed, C., Evans, M. J., Di Carlo, P., Lee, J. D., and Carpenter, L. J.: Interferences in photolytic NO₂ measurements: explanation for an apparent missing oxidant?, *Atmos. Chem. Phys.*, 16, 4707-4724, doi:10.5194/acp-16-4707-2016, 2016b.
- 755 Roberts, J. M.: The atmospheric chemistry of organic nitrates, *Atmos. Environ. A-Gen.*, 24, 243-287, doi:10.1016/0960-1686(90)90108-Y, 1990.
- Roberts, J. M., Williams, J., Baumann, K., Buhr, M. P., Goldan, P. D., Holloway, J., Hübler, G., Kuster, W. C., McKeen, S. A., Ryerson, T. B., et al.: Measurements of PAN, PPN, and MPAN made during the 1994 and 1995 Nashville Intensives of the Southern Oxidant Study: Implications for regional ozone production from biogenic hydrocarbons, *J. Geophys. Res.-Atmos.*, 103, 22473-22490, doi:10.1029/98JD01637, 1998.
- 760 Roberts, J. M., Flocke, F., Stroud, C. A., Hereid, D., Williams, E., Fehsenfeld, F., Brune, W., Martinez, M., and Harder, H.: Ground-based measurements of peroxy-carboxylic nitric anhydrides (PANs) during the 1999 Southern Oxidants Study Nashville Intensive, *J. Geophys. Res.-Atmos.*, 107, ACH 1-1-ACH 1-10, doi:10.1029/2001JD000947, 2002.
- 765 Ryerson, T. B., Williams, E. J., and Fehsenfeld, F. C.: An efficient photolysis system for fast-response NO₂ measurements, *J. Geophys. Res.-Atmos.*, 105, 26447-26461, doi:10.1029/2000JD900389, 2000.
- Schultz, M. G., Jacob, D. J., Wang, Y., Logan, J. A., Atlas, E. L., Blake, D. R., Blake, N. J., Bradshaw, J. D., Browell, E. V., Fenn, M. A., et al.: On the origin of tropospheric ozone and NO_x over the tropical South Pacific, *J. Geophys. Res.: Atmos.*, 104, 5829-5843, doi:10.1029/98jd02309, 1999.

- 770 Seltzer, K. M., Vizuete, W., and Henderson, B. H.: Evaluation of updated nitric acid chemistry on ozone precursors and radiative effects, *Atmos. Chem. Phys.*, 15, 5973-5986, doi:10.5194/acp-15-5973-2015, 2015.
- Shah, V., Jacob, D. J., Dang, R., Lamsal, L. N., Strode, S. A., Steenrod, S. D., Boersma, K. F., Eastham, S. D., Fritz, T. M., Thompson, C., et al.: Nitrogen oxides in the free troposphere: implications for tropospheric oxidants and the interpretation of satellite NO₂ measurements, *Atmos. Chem. Phys.*, 23, 1227-1257, doi:10.5194/acp-23-1227-2023, 2023.
- 775 Silvern, R. F., Jacob, D. J., Travis, K. R., Sherwen, T., Evans, M. J., Cohen, R. C., Laughner, J. L., Hall, S. R., Ullmann, K., Crounse, J. D., et al.: Observed NO/NO₂ Ratios in the Upper Troposphere Imply Errors in NO-NO₂-O₃ Cycling Kinetics or an Unaccounted NO_x Reservoir, *Geophys. Res. Lett.*, 45, 4466-4474, doi:10.1029/2018gl077728, 2018.
- 780 Singh, H. B.: Reactive nitrogen in the troposphere, *Environ. Sci. Technol.*, 21, 320-327, doi:10.1021/es00158a001, 1987.
- Singh, H. B., Thompson, A. M., and Schlager, H.: SONEX airborne mission and coordinated POLINAT-2 activity: Overview and accomplishments, *Geophys. Res. Lett.*, 26, 3053-3056, doi:10.1029/1999GL900588, 1999.
- 785 Singh, H. B., Brune, W. H., Crawford, J. H., Jacob, D. J., and Russell, P. B.: Overview of the summer 2004 Intercontinental Chemical Transport Experiment–North America (INTEX-A), *J. Geophys. Res.-Atmos.*, 111, doi:10.1029/2006JD007905, 2006.
- Singh, H. B., Brune, W. H., Crawford, J. H., Flocke, F., and Jacob, D. J.: Chemistry and transport of pollution over the Gulf of Mexico and the Pacific: spring 2006 INTEX-B campaign overview and first results, *Atmos. Chem. Phys.*, 9, 2301-2318, doi:10.5194/acp-9-2301-2009, 2009.
- 790 Sörgel, M., Regelin, E., Bozem, H., Diesch, J. M., Drewnick, F., Fischer, H., Harder, H., Held, A., Hosaynali-Beygi, Z., Martinez, M., et al.: Quantification of the unknown HONO daytime source and its relation to NO₂, *Atmos. Chem. Phys.*, 11, 10433-10447, doi:10.5194/acp-11-10433-2011, 2011.
- Stettler, M. E. J., Eastham, S., and Barrett, S. R. H.: Air quality and public health impacts of UK airports. Part I: Emissions, *Atmos. Environ.*, 45, 5415-5424, doi:10.1016/j.atmosenv.2011.07.012, 2011.
- 795 Stratmann, G., Ziereis, H., Stock, P., Brenninkmeijer, C. A. M., Zahn, A., Rauthe-Schöch, A., Velthoven, P. V., Schlager, H., and Volz-Thomas, A.: NO and NO_y in the upper troposphere: Nine years of CARIBIC measurements onboard a passenger aircraft, *Atmos. Environ.*, 133, 93-111, doi:10.1016/j.atmosenv.2016.02.035, 2016.
- 800 Talbot, R. W., Dibb, J. E., Scheuer, E. M., Kondo, Y., Koike, M., Singh, H. B., Salas, L. B., Fukui, Y., Ballenthin, J. O., Meads, R. F., et al.: Reactive nitrogen budget during the NASA SONEX Mission, *Geophys. Res. Lett.*, 26, 3057-3060, doi:10.1029/1999GL900589, 1999.
- The International GEOS-Chem User Community: <https://doi.org/10.5281/zenodo.4681204>, 2021.
- 805 Thomas, K., Berg, M., Boulanger, D., Houben, N., Gressent, A., Nédélec, P., Pätz, H.-W., Thouret, V., and Volz-Thomas, A.: Climatology of NO_y in the troposphere and UT/LS from measurements made in MOZAIC, *Tellus B*, 67, 28793, doi:10.3402/tellusb.v67.28793, 2015.
- Thompson, C. R., Wofsy, S. C., Prather, M. J., Newman, P. A., Hanisco, T. F., Ryerson, T. B., Fahey, D. W., Apel, E. C., Brock, C. A., Brune, W. H., et al.: The NASA Atmospheric Tomography (ATom) Mission: Imaging the chemistry of the global atmosphere, *B. Am. Meteorol. Soc.*, 1-53, doi:10.1175/bams-d-20-0315.1, 2021.

- 810 Toon, O. B., Maring, H., Dibb, J., Ferrare, R., Jacob, D. J., Jensen, E. J., Luo, Z. J., Mace, G. G., Pan, L. L., Pfister, L., et al.: Planning, implementation, and scientific goals of the Studies of Emissions and Atmospheric Composition, Clouds and Climate Coupling by Regional Surveys (SEAC⁴RS) field mission, *J. Geophys. Res.-Atmos.*, 121, 4967-5009, doi:10.1002/2015jd024297, 2016.
- 815 Travis, K. R., Jacob, D. J., Fisher, J. A., Kim, P. S., Marais, E. A., Zhu, L., Yu, K., Miller, C. C., Yantosca, R. M., Sulprizio, M. P., et al.: Why do models overestimate surface ozone in the Southeast United States?, *Atmos. Chem. Phys.*, 16, 13561-13577, doi:10.5194/acp-16-13561-2016, 2016.
- Travis, K. R., Heald, C. L., Allen, H. M., Apel, E. C., Arnold, S. R., Blake, D. R., Brune, W. H., Chen, X., Commane, R., Crounse, J. D., et al.: Constraining remote oxidation capacity with ATom observations, *Atmos. Chem. Phys.*, 20, 7753-7781, doi:10.5194/acp-20-7753-2020, 2020.
- 820 Travis, K. R., Nault, B. A., Crawford, J. H., Bates, K. H., Blake, D. R., Cohen, R. C., Fried, A., Hall, S. R., Huey, L. G., Lee, Y. R., et al.: Impact of improved representation of VOC emissions and production of NO_x reservoirs on modeled urban ozone production, *Atmos. Chem. Phys.*, 2024, 1-27, doi:10.5194/egusphere-2024-951, 2024.
- 825 Volz-Thomas, A., Berg, M., Heil, T., Houben, N., Lerner, A., Petrick, W., Raak, D., and Pätz, H. W.: Measurements of total odd nitrogen (NO_y) aboard MOZAIC in-service aircraft: instrument design, operation and performance, *Atmos. Chem. Phys.*, 5, 583-595, doi:10.5194/acp-5-583-2005, 2005.
- Weinheimer, A. J., Walega, J. G., Ridley, B. A., Gary, B. L., Blake, D. R., Blake, N. J., Rowland, F. S., Sachse, G. W., Anderson, B. E., and Collins, J. E.: Meridional distributions of NO_x, NO_y, and other species in the lower stratosphere and upper troposphere during AASE II, *Geophys. Res. Lett.*, 21, 2583-2586, doi:10.1029/94GL01897, 1994.
- 830 Weinheimer, A. J.: Chemical Methods: Chemiluminescence, Chemical Amplification, Electrochemistry, and Derivation, in: *Analytical Techniques for Atmospheric Measurement*, 311-360, doi:10.1002/9780470988510.ch7, 2006.
- 835 Worden, H. M., Bowman, K. W., Kulawik, S. S., and Aghedo, A. M.: Sensitivity of outgoing longwave radiative flux to the global vertical distribution of ozone characterized by instantaneous radiative kernels from Aura-TES, *J. Geophys. Res.*, 116, doi:10.1029/2010jd015101, 2011.
- Zahn, A., Brenninkmeijer, C. A. M., Asman, W. A. H., Crutzen, P. J., Heinrich, G., Fischer, H., Cuijpers, J. W. M., and van Velthoven, P. F. J.: Budgets of O₃ and CO in the upper troposphere: CARIBIC passenger aircraft results 1997–2001, *J. Geophys. Res.-Atmos.*, 107, ACH 6-1-ACH 6-20, doi:10.1029/2001JD001529, 2002.

840